

10  
199-960881

CONF-9605173--4

SLAC-PUB-7158  
April, 1996

# Measurement of Subpicosecond Electron Pulse Length\*

Hung-chi Lihrn<sup>1</sup>

*Applied Physics Department and Stanford Linear Accelerator Center,  
Stanford University, Stanford, California 94305*

**Abstract.** A new frequency-resolved bunch-length measuring system has been developed at the Stanford SUNSHINE facility to characterize subpicosecond electron pulses. Using a far-infrared Michelson interferometer, this method measures the spectrum of coherent transition radiation emitted from electron bunches through optical autocorrelation. The electron bunch length is obtained from the measurement with a simple and systematic analysis which includes interference effects caused by the beam splitter. This method demonstrates subpicosecond resolving power that cannot be achieved by existing time-resolved methods. The principle of this method and experimental results are discussed.

## INTRODUCTION

In the recent development of particle accelerators, the production of very short electron bunches has become an interesting direction. Many future accelerators designs such as next-generation synchrotron light sources, future linear colliders, free-electron lasers, and high-intensity coherent far-infrared light sources demand electron bunches of subpicosecond duration. Hence, a bunch-length measuring system capable of characterizing subpicosecond pulses will provide a powerful diagnostic tool to assist this development.

As a direct approach, a time-resolved method, which resolves the beam-generated signal in the time domain, is normally applied to measure the bunch length. However, existing fast time-resolved methods such as the streak camera can not provide enough resolution for subpicosecond electron pulses, and

\*Work supported by Department of Energy contract DE-AC03-76SF00515.  
<sup>1</sup>Present address: Tencor Instruments, 2400 Charleston Road, Mountain View, California 94043

*Presented for the 1996 Faraday Cup Award  
at the 7th Beam Instrumentation Workshop,  
Argonne, Illinois, May 6-9, 1996.*

the hardware has already become very complicated and expensive. In contrast, a frequency-resolved technique, which extracts the frequency content of a beam-generated signal, does not require fast processing speed and complex hardware. From the frequency information, the particle distribution can be deduced. Since the necessary broad bandwidth required for subpicosecond pulses can be achieved by optical methods, a good subpicosecond resolution can be easily obtained. This is a well-known technique used in the characterization of femtosecond laser pulses(1) and has been suggested for electron bunch-length measurements(2).

## PRINCIPLE OF AUTOCORRELATION METHOD

This frequency-resolved method uses a far-infrared Michelson interferometer to measure the spectrum of coherent transition radiation through optical autocorrelation. Coherent transition radiation emitted from electron pulses carries the information of bunch distribution in its frequency content. By analyzing the frequency information, the bunch length can be derived.

### Coherent Transition Radiation

Transition radiation is generated when an electron passes the interface of two media of different dielectric constants(6). For a vacuum-metal interface, the spectrum of transition radiation is approximately flat in the far-infrared regime due to the almost perfect conductivity of the metal. The radiated intensity from a relativistic electron has a zero at  $\theta = 0$  and reaches maximum at  $\theta \sim 1/\gamma$ , where  $\theta$  is the angle between the radiation and the electron direction, and  $\gamma$  is the Lorentz factor(5-7).

When a bunch of  $N$  electrons passes the interface, the resulting total intensity at angular frequency  $\omega$  can be expressed as(8)

$$I_{\text{total}}(\omega) = N|1 + (N-1)f(\omega)|I_e(\omega), \quad (1)$$

where  $I_e(\omega)$  is the intensity of transition radiation emitted by an electron at frequency  $\omega$ . In the far-infrared regime,  $I_e(\omega)$  is constant. The form factor  $f(\omega)$  is given by the three-dimensional Fourier transform of the electron bunch distribution(5,7,8). If the radiation can be observed in the forward direction ( $\theta = 0$ ) from a transversely symmetric beam, the form factor  $f(\omega)$  is only determined by the longitudinal bunch distribution.

MASTER

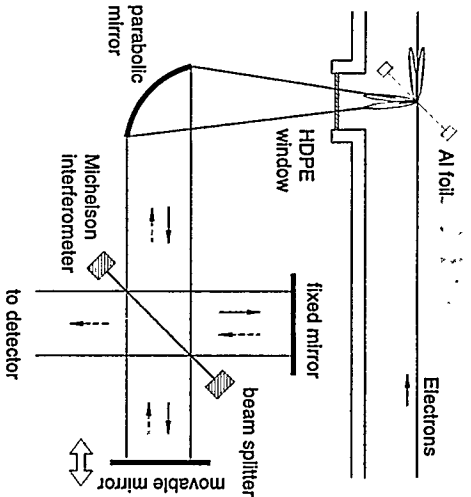


FIGURE 1. Schematic diagram of a Michelson interferometer for bunch-length measurements.

However, transition radiation does not produce radiation in the forward direction. In order to use transition radiation to measure the bunch length, observing the radiation in an off-axis direction ( $\theta \neq 0$ ) is necessary. In this case, the transverse bunch distribution will contribute to the form factor even for a transversely symmetric beam. For large angles or big transverse beam sizes, the transverse contribution will result in an apparent bunch-length measurement that is longer than the actual one(5,7). This transverse contribution, however, can be ignored if the condition  $\rho \ll l$  is satisfied, where  $\rho$  is the transverse beam size, and  $l$  is the bunch length(5,7). This condition is assumed in the following analysis and is automatically obtained when the beam conditions are optimized in experiments. Hence, proper focusing to produce small transverse beam size and a reasonable angular acceptance for the detector is crucial for accurate subpicosecond bunch-length measurements.

#### Far-infrared Michelson Interferometer

Since the spectrum of coherent transition radiation emitted by subpicosecond electron bunches is in the far-infrared regime(4,7), a far-infrared Michelson interferometer shown in Fig. 1 is used to measure the spectrum via optical autocorrelation. It consists of a beam splitter, a fixed and a movable mirror, and a detector. When light enters the Michelson interferometer, the beam splitter splits its amplitude into two mirror arms. As these two rays are reflected from the mirrors, they are recombined at the beam splitter and sent into the detector.

An ideal beam splitter has constant amplitude reflection ( $R$ ) and transmis-

sion ( $T$ ) coefficients over all frequencies, which satisfy  $|R|^2 = |T|^2 = 1/2$ . As shown in Fig. 1, for an incoming light pulse of electric field  $E$  with intensity proportional to  $|E|^2$ , the light pulse split by the beam splitter and reflected by the fixed mirror has a field amplitude of  $T(RE)$  when it reaches the detector; on the other hand, the light pulse reflected by the movable mirror has an amplitude of  $R(TE)$  at the detector. Perfect reflection on the mirrors is assumed. At zero optical path difference, the pulses completely overlap at the detector, and the total intensity reaches the maximum  $|2RTE|^2 = |E|^2$ . As the path difference increases but is still shorter than the bunch length, the two pulses overlap partially, and the total intensity decreases. When the path difference of two arms is larger than the bunch length, the two pulses are totally separated in time, and the resulting intensity at the detector is  $2|RT|^2|E|^2/2$ . The intensity is constant over all path differences greater than the bunch length and is called the *baseline*. The variation of intensity about the baseline as a function of optical path difference is called the *interferogram*. Therefore, the width of the peak in the interferogram can be used to measure the bunch length.

The intensity of the recombined radiation at the detector can be expressed in the time domain with an additional time delay  $\delta/c$  for the movable arm by

$$\begin{aligned}
 I(\delta) &\propto \int_{-\infty}^{+\infty} |TRE(t) + RTE(t + \frac{\delta}{c})|^2 dt \\
 &= \underbrace{2|RT|^2 \operatorname{Re} \int_{-\infty}^{+\infty} E(t)E^*(t + \frac{\delta}{c}) dt}_{S(\delta)} + \underbrace{2|RT|^2 \int_{-\infty}^{+\infty} |E(t)|^2 dt}_{I_{\infty}}, \quad (2)
 \end{aligned}$$

or in the frequency domain with a phase factor  $e^{-i\omega\delta/c}$  for the movable arm by

$$\begin{aligned}
 I(\delta) &\propto \int_{-\infty}^{+\infty} |TRE(\omega) + RTE(\omega)e^{-i\omega\delta/c}|^2 d\omega \\
 &= \underbrace{2 \operatorname{Re} \int_{-\infty}^{+\infty} |RT|^2 |\tilde{E}(\omega)|^2 e^{-i\omega\delta/c} d\omega}_{S(\delta)} + \underbrace{2 \int_{-\infty}^{+\infty} |RT|^2 |\tilde{E}(\omega)|^2 d\omega}_{I_{\infty}}, \quad (3)
 \end{aligned}$$

where  $\delta$  is the optical path difference,  $c$  is the speed of light,  $S(\delta)$  denotes the interferogram, and  $I_{\infty}$  is the baseline defined as the intensity at  $\delta \rightarrow \pm\infty$ . Equations (2) and (3) are related by the Fourier transform  $\tilde{E}(\omega) = \frac{1}{\sqrt{2\pi}} \int_{-\infty}^{+\infty} E(t)e^{i\omega t} dt$ . Therefore, the interferogram  $S(\delta)$  is the autocorrelation of the incident light pulse [cf. Eq. (2)], and its Fourier transform is the power spectrum of the pulse [cf. Eq. (3)]. Solving for  $|\tilde{E}(\omega)|^2$  in Eq. (3) and using Eq. (1) with the relation  $I_{\text{total}}(\omega) \propto |\tilde{E}(\omega)|^2$ , the bunch form factor can be obtained by

$$f(\omega) \propto \frac{1}{N-1} \left[ \frac{1}{4\pi c |RT|^2 N I_{\infty}(\omega)} \int_{-\infty}^{+\infty} S(\delta) e^{i\omega\delta/c} d\delta - 1 \right], \quad (4)$$

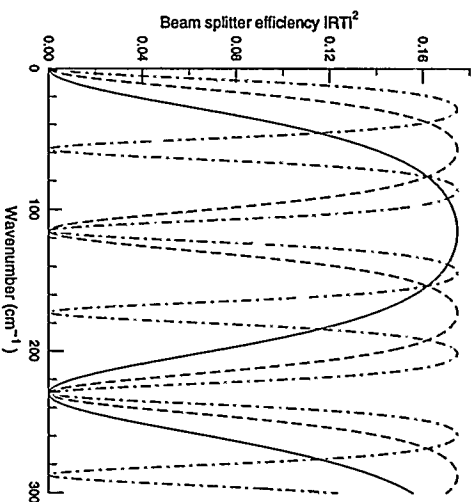


FIGURE 2. The efficiency of Mylar beam splitter as a function of frequency for different thicknesses: 12.7 (solid), 25.4 (dashed), and 50.8  $\mu\text{m}$  (dash-dotted line).

where  $|\tilde{E}(\omega)|^2 = |\tilde{E}(-\omega)|^2$  is used since  $E(t)$  is a real function. Hence, the interferogram contains the frequency spectrum of coherent transition radiation and can be used to derive the bunch length.

### Mylar Beam-splitter Interference Effects

Suitable beam splitters for the far-infrared regime (a Mylar foil in our design) do not provide constant and equal reflectance and transmittance for all frequencies. This is caused by the interference of light reflected from both surfaces of the beam splitter, which is equivalent to thin-film interference in optics(9). The total amplitude reflection and transmission coefficients for a Mylar foil of thickness  $t$  and refractive index  $n$  mounted at a  $45^\circ$  angle to the direction of incoming light are given respectively by(7,10)

$$R = -r \frac{1 - e^{i\phi}}{1 - r^2 e^{i\phi}} \quad \text{and} \quad T = (1 - r^2) \frac{e^{i\phi/2}}{1 - r^2 e^{i\phi}}, \quad (5)$$

where  $r$  is the amplitude reflection coefficient of the air-to-Mylar interface at a  $45^\circ$  incident angle, and  $\phi$  is defined as  $4\pi t n \sqrt{n^2 - (1/2)^2}$  at wavenumber  $\sigma = \omega/2\pi c$ (7,11). No absorption in the foil is assumed, and the refractive index is assumed to be constant ( $n = 1.85$ ) over all frequencies(11).

The efficiency of the beam splitter defined as  $|RT|^2$  is shown in Fig. 2. The efficiency becomes zero at frequencies where light reflected from both surfaces of the beam splitter interferes destructively. Derivations in the time domain such as Eq. (2) are no longer valid for varying efficiency; however, those in the

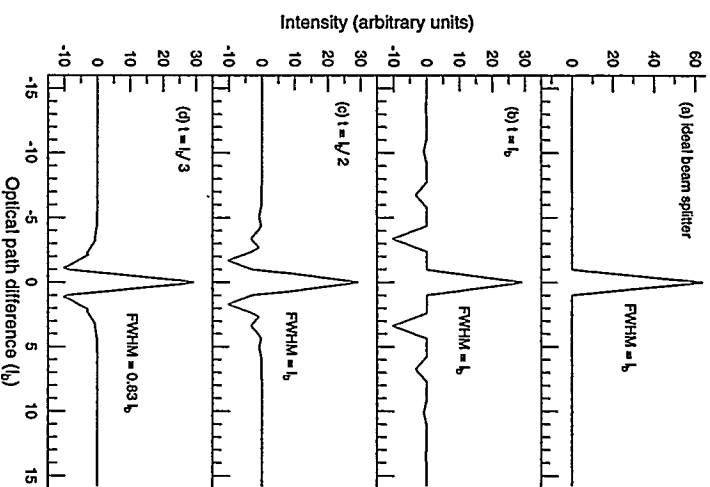


FIGURE 3. The simulation of the beam-splitter interference effects on a rectangular bunch distribution with different beam splitters: (a) an ideal beam splitter and Mylar beam splitters of thicknesses (t) (b) equal to, (c) half, and (d) one third of the bunch length ( $l_b$ ).

frequency domain such as Eq. (3) still hold. The width of the interferogram can not be directly used for bunch-length estimation unless interference effects on the interferogram are included.

### Bunch-length Analysis

The interference effects are studied numerically for both Gaussian and rectangular bunch distributions, and the bunch length is then derived from this study. Although real bunch distributions are neither Gaussian nor rectangular, the bunch lengths deduced from the two distributions will give reasonable bounds for the real one.

Examples of the beam-splitter interference effects on a rectangular bunch distribution are shown in Fig. 3. For an ideal beam splitter, the interferogram has the expected triangular peak with its FWHM equal to the bunch length [cf. Fig. 3(a)]. For Mylar beam splitters, negative valleys appear in the interferograms, which are due to suppression of the low frequency area by the

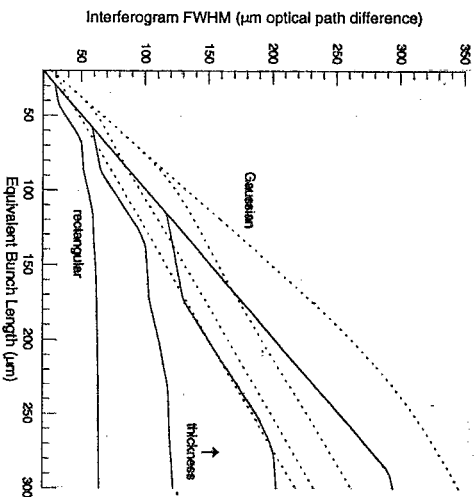


FIGURE 4. Interferogram FWHM's as functions of equivalent bunch lengths of both Gaussian (dotted lines) and rectangular (solid lines) bunch distributions for different Mylar beam-splitter thicknesses: 12.7, 25.4, 50.8, and 127  $\mu\text{m}$ . Within the same distribution, the lines are shown from the bottom to the top in the increasing order of thickness.

first zero of the beam-splitter efficiency. These valleys move closer to the main peak as the beam-splitter thickness ( $t$ ) decreases [cf., Fig. 3(b)-(d)]. For beam splitters thinner than about half the bunch length ( $t_b$ ), they merge with the main peak and narrows the peak [cf., Fig. 3(d)]. The effects are similar for a Gaussian distribution. Detailed results on how the FWHM values of the interferogram change with the bunch length for both Gaussian and rectangular distributions are shown in Fig. 4. Once the beam splitter is chosen, the bunch length can be derived from the measured interferogram width through Fig. 4.

### EXPERIMENTAL SETUP

To demonstrate this method, the SUNSHINE facility was operated to produce 1- $\mu$  pulse trains at 10 Hz containing about 3000 electron bunches at an energy of 30 MeV. Each bunch had about  $3.5 \times 10^7$  electrons. As shown in Fig. 1, transition radiation is generated when the electrons pass through an Al foil. The divergent backward transition radiation is extracted from the evacuated beam line into air via a high-density polyethylene (HDPE) window and is converted into parallel light by an off-axis paraboloidal mirror(12). The parallel light then enters a far-infrared Michelson interferometer.

The interferometer consists of a Mylar beam splitter mounted at a 45° angle to the direction of incident light, a fixed and a movable first-surface mirror,

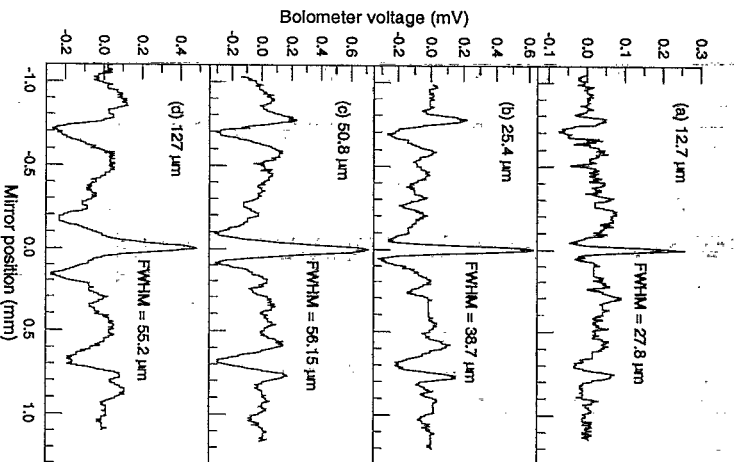


FIGURE 5. Interferograms measured for different Mylar beam-splitter thicknesses: (a) 12.7, (b) 25.4, (c) 50.8, and (d) 127  $\mu\text{m}$ . The FWHM's of the main peaks are measured in mirror movement, which are half of widths in optical path difference.

and a room-temperature detector. The movable mirror is moved by a linear actuator via a PC. The detector consists of a Moletron P1-65 LiTaO<sub>3</sub> pyroelectric bolometer and a pre-amplifier(3,4,12). The detector signal is digitized into the computer. With the computer interfaces, the autocorrelation measurements are performed automatically through the program under the LabVIEW control environment implemented on the computer.

### RESULTS AND DISCUSSION

By measuring the detector signal as a function of the position of the movable mirror via the computer program, the interferograms of 2.2 mm long with 5- $\mu$ m mirror step size are measured for four different Mylar beam-splitter thicknesses and shown in Fig. 5. This 5- $\mu$ m mirror step size corresponding to a 33-fs time resolution is good enough for the measurements; however, a subfemtosecond resolution can still be achieved by the actuator with a submicron step size. The beam parameters are kept the same when different beam splitters are

**TABLE 1.** Measured interferogram FWHM's in optical path difference (OPD) for different beam-splitter thicknesses and the corresponding estimated equivalent bunch lengths deduced from Fig. 4 for Gaussian and rectangular distributions.

Beam splitter thickness ( $\mu\text{m}$ )	Interferogram FWHM		Estimated equivalent bunch length ( $\mu\text{m}$ )	
	OPD ( $\mu\text{m}$ )	Gaussian	Rectangular	
12.7	55.6	60.8	100.6	
25.4	77.4	72.8	103.2	
50.8	112.3	86.9	111.0	
127.0	110.4	83.1	109.1	

used. The valleys around the main peak are separated farther apart as the beam-splitter thickness increases. This widens the main peak [cf., Fig. 5(a)-(c)] until the valleys are out of the peak [cf., Fig. 5(c),(d)]. The base of the peak can even be seen in Fig. 5(d). The measured interferogram FWHM's and the estimated equivalent bunch lengths deduced from Fig. 4 for Gaussian and rectangular distributions are shown in Table 1. The estimated bunch lengths provide bounds for the real bunch length and are consistent over a 10-fold change in the beam-splitter thickness. The real bunch length is estimated about  $100 \mu\text{m}$  ( $0.33 \text{ ps}$ ) long.

Non-destructive methods such as using a bending magnet to generate coherent synchrotron radiation and using a metal foil with a hole to generate coherent diffraction radiation are suitable for applications where keeping good beam quality is essential. Unlike the case for transition radiation, the single-electron spectrum of these radiating processes is not constant in frequency. In order to extract bunch information  $f(\omega)$ , the measured spectrum has to be numerically corrected for the single-electron spectrum  $I_e(\omega)$ .

In principle, the measured spectral information can be used to reconstruct the bunch distribution and give a better bunch-length measurement. However, there are some practical difficulties in reconstructing the electron distribution for this experiment. The spectrum is contaminated by water absorption lines caused by humidity in ambient air (4), and the zeros of the beam-splitter efficiency produce artifacts when the spectrum is numerically corrected for the beam-splitter interference effects (4). Although one-dimensional phase-retrieval methods have been suggested for this reconstruction problem (13,14), they can not guarantee the uniqueness of the solution (7). Alternatively, a new method described in Ref. (7) using two-dimensional autocorrelation scans with a three-dimensional phase-retrieval method may be used to obtain the three-dimensional bunch distribution with the guaranteed uniqueness of the solution.

## CONCLUSION

In conclusion, a new frequency-resolved bunch-length measuring method suitable for subpicosecond electron pulses has been developed at the SUNSHINE facility. This method measures the autocorrelation of coherent transition radiation emitted from electron bunches through a far-infrared Michelson interferometer. Measurements have verified this method by showing consistent results over a broad range of beam-splitter thicknesses. Based on a low-cost, easy-to-operate, compact, and transportable Michelson interferometer, this autocorrelation method demonstrates a subpicosecond resolving power far better than existing time-resolved methods.

## ACKNOWLEDGEMENT

The author would like to thank Prof. H. Wiedemann at Stanford University for his advise and support of this work. Thanks also go to D. Bocek, P. Kung, J. Sebek, C. Settakorn, and R. Theobald for their technical assistance. This work is supported by Department of Energy (contract No. DE-AC03-76SF00515).

## REFERENCES

1. Fork, R. L., Greene, B. I., and Shank, C. V., *Appl. Phys. Lett.* **38**, 671 (1981).
2. Barry, W., in *Proceedings of the Workshop on Advanced Beam Instrumentation I*, KEK, Tsukuba, Japan, April 22-24, 1991 (unpublished).
3. Kung, P., Lihn, H.-C., Bocek, D., and Wiedemann, H., *Proc. SPIE* **2118**, 191 (1994).
4. Kung, P., Lihn, H.-C., Bocek, D., and Wiedemann, H., *Phys. Rev. Lett.* **73**, 967 (1994).
5. Lihn, H.-C., Kung, P., Settakorn, C., Bocek, D., and Wiedemann, H., *Phys. Rev. E*, to be published.
6. Ginsburg, V. L., and Frank, I. M., *Zh. Eksp. Teor. Fiz.* **16**, 15 (1946).
7. Lihn, H.-C., *Stimulated Coherent Transition Radiation*, Ph.D. thesis, Stanford University, Stanford, 1996.
8. Nodvic, J. S., and Saxon, D. S., *Phys. Rev.* **96**, 180 (1954).
9. Hecht, E., and Zajac, A., *Optics*, Addison-Wesley, Reading, Massachusetts, 1974, Sec. 9.7.
10. Chantry, G. W., *Submillimetre Spectroscopy*, Academic Press, London, 1971, App. A.
11. Bell, R. J., *Introductory Fourier Transform Spectroscopy*, Academic Press, London, 1972, Ch. 9.
12. Lihn, H.-C., Kung, P., Bocek, D., and Wiedemann, H., *AIP Conference Proceedings* **333**, 231 (1995).
13. Fienup, J. R., *Opt. Lett.* **3**, 27 (1978).
14. Lai, R., Hapke, U., and Sievers, J., *Phys. Rev. E* **50**, R4294 (1994).

## **DISCLAIMER**

This report was prepared as an account of work sponsored by an agency of the United States Government. Neither the United States Government nor any agency thereof, nor any of their employees, makes any warranty, express or implied, or assumes any legal liability or responsibility for the accuracy, completeness, or usefulness of any information, apparatus, product, or process disclosed, or represents that its use would not infringe privately owned rights. Reference herein to any specific commercial product, process, or service by trade name, trademark, manufacturer, or otherwise does not necessarily constitute or imply its endorsement, recommendation, or favoring by the United States Government or any agency thereof. The views and opinions of authors expressed herein do not necessarily state or reflect those of the United States Government or any agency thereof.

**DISCLAIMER**

**Portions of this document may be illegible in electronic image products. Images are produced from the best available original document.**